Progress in PHOTOVOLTAICS

PROGRESS IN PHOTOVOLTAICS: RESEARCH AND APPLICATIONS
Prog. Photovolt: Res. Appl. 2015; **23**:1144–1156
Published online 19 July 2014 in Wiley Online Library (wileyonlinelibrary.com). DOI: 10.1002/pip.2533

RESEARCH ARTICLE

Broadband absorption enhancement in ultra-thin crystalline Si solar cells by incorporating metallic and dielectric nanostructures in the back reflector

Samarth Jain[1,3], Valerie Depauw[1], Vladimir D. Miljkovic[2], Alexander Dmitriev[2], Christos Trompoukis[1], Ivan Gordon[1], Pol Van Dorpe[1] and Ounsi El Daif[1,4]*

[1] PV, IMEC, Leuven, Belgium
[2] Chalmers University of Technology, Gottenburg, Sweden
[3] Now at Silhouette Rainbows, Sikandra, Agra, India
[4] Now at Qatar Environment and Energy Research Center (QEERI), Qatar Foundation, Doha, Qatar

ABSTRACT

We propose a back reflecting scheme in order to enhance the maximum achievable current in one micron thick crystalline silicon solar cells. We perform 3D numerical investigations of the scattering properties of metallic nanostructures located at the back side and optimize them for enhancing absorption in the silicon layer. We validate our numerical results experimentally and also compare the absorption enhancement in the solar cell structure, both with quasi-periodic and random metallic nanostructures. We have looked at the interplay between the metallic nanostructures and an integrated back reflector. We show that the combination of metallic nanoparticles and a metallic reflector results in significant parasitic absorption. We compared this to another implementation based on titanium dioxide nanoparticles, which act as a Lambertian reflector of light. Our simulation and experimental results show that this proposed configuration results in reduced absorption losses and in broadband enhancement of absorption for ultra-thin solar cells, paving the way to an optimal back reflector for thin film photovoltaics. Copyright © 2014 John Wiley & Sons, Ltd.

KEYWORDS

plasmons; solar cells; optics; crystalline silicon; nanoparticles

***Correspondence**

O. El Daif, Qatar Environment and Energy Research Institute (QEERI), Qatar Foundation, Doha, Qatar.
E-mail: oeldaif@qf.org.qa

Received 19 March 2013; Revised 23 November 2013; Accepted 2 June 2014

1. INTRODUCTION

Ultra-thin film (<5 μm) and thin film (<100 μm) crystalline silicon solar cells are promising solutions for the issue of high production costs of solar cells. Ultra-thin film (<5 μm) cells, besides the cost-reduction advantage, offer various advantages such as faster production, higher open circuit voltage [1], and enhanced charge collection efficiency [2].

However, with reduced thickness of the crystalline silicon (c-Si) layer, absorption decreases considerably because of the low absorption coefficient of c-Si (because of its indirect band gap); it requires ~1 mm of c-Si to completely absorb light of 1100 nm wavelength, and this results in low efficiency of thin film solar cells. Thus, as we go toward thinner substrates, the importance of light trapping increases significantly. Currently, to address the problem of low light absorption in standard industrial solar cell structures (~thickness 180 μm), solutions such as anti reflection coatings (ARCs) and surface texturing at micron scale are used. Typical surface texturing has a feature size of 10–15 μm and around the same thickness of the material [3] is lost, making it unsuitable for application in thin film and ultra-thin film solar cells. Some groups have proposed submicron surface texturing [4–6]; however, this results in very high surface roughness, and hence, it enhances losses because of surface recombination. As for ARCs, they are not sufficient for increasing absorption in thin film cells, for they only enhance transmission around their resonance wavelength. But as the semiconductor layer is thin, light is not fully absorbed in one pass, and it needs to be redirected back to the semiconductor in an efficient manner.

Ever since the path breaking work of Michael Faraday [7] on the problem of color of colloidal gold solution, there has been growing interest in optical properties and behavior of

metallic structures at nanoscale. Noble metal nanostructures are known to support localized surface plasmons [8], that is, electromagnetic modes arising at the interface between a metal and a dielectric. This plasmonic behavior arises because of the collective oscillation of confined conduction electrons with the incident electromagnetic wave. For structures having dimensions smaller than the wavelength of light impinging on them, the conduction electrons start oscillating in phase, resulting in charge polarization at the surface. This charge polarization builds up a restoring force, which sustains the resonance at specific wavelengths, giving rise to a resonantly enhanced field throughout the particle and also outside of it. This results in large scattering and absorption cross section of plasmonic metallic nanoparticles and enhances the electric field in the surroundings. The plasmonic behavior, damping and strength of the plasmonic excitation, is a function of the shape, size, and material of the particle, of the dielectric function of the surrounding medium and nearby material [9] and can thus be tuned to the desired spectral range. Incorporation of plasmonic metallic nanostructures has the potential to overcome the problem of light trapping in ultra-thin film solar cells by reducing reflection or by redirecting light toward silicon in efficient manner and is a widely studied field [10,11]. Two main approaches applied for using the plasmonic particles depending on the cell architecture and material for solar cells are as follows: (i) incorporating the plasmonic nanoparticles directly into the semiconductor layer, an approach that takes advantage of the near field enhancement [12] and (ii) using the plasmonic nanoparticle on the front or the back side of the solar cells, an approach that employs the resonant scattering property of plasmons along with their directional scattering property [13].

Earlier studies suggested that using plasmonic nanostructures at the front side of the solar cell results in a decrease in its energy-conversion efficiency [14,15]. The reason attributed to this is that, for frequencies greater than the plasmon resonance of the metal nanoparticles, the destructive interference between transmitted and scattered electromagnetic wave results in Fano resonance, causing an increase in reflection [16,17] and hence reducing the external quantum efficiency. To avoid this loss, the trend has shifted from using the plasmonic nanostructure at the front to using them at the back, which uses preferential scattering properties. Preferential scattering phenomena arise when the near field around the dipole interacts with the high index surrounding. The closer the particle is to the high index material, the larger the asymmetry is in the angular distribution of scattered light, thus enabling us to use the particles at the back side configuration and scatter light toward the semiconducting layer.

In this study, we address both the problem of low light absorption in ultra-thin substrates and of parasitic/Ohmic absorption in the flat metal back reflector. Firstly, we optimize the back reflector architecture by employing metallic nanostructures that exhibit plasmonic characteristics, so as to scatter light back into silicon. We then replace the flat metallic back reflector (i.e., flat aluminum layer) by a dielectric back surface reflector for diffusively reflecting light back toward silicon, thus having the advantage of randomizing the direction of reflected light and also avoiding any parasitic absorption as in the case of the flat metallic back reflector.

2. METHODS AND TECHNIQUES

2.1. Structures chosen

We use one-micron-thick epifree crystalline silicon (c-Si) layers on glass, developed in house [18]. This technology gives the possibility of fabricating solar cells on exceptionally thin monocrystalline silicon films [19]. The silicon layer is bonded to a transparent superstrate after deposition of an antireflection coating, and contacting is therefore completely done through the rear.

In order to isolate the effect of the back reflector, we first studied the effect of the plasmonic nanostructures on a minimal stack of silicon on glass with intermediate ARC. Once we studied its effect and optimized it for absorption enhancement, we extrapolated and adapted the optimal back reflecting structure to an active solar cell stack, with a 40 nm SiNx antireflection coating and a back side heterojunction emitter stack (amorphous Si and indium tin oxide [ITO] [19]).

In each case, we use as a reference the planar structure (either silicon alone or the cell stack) with an aluminum metal reflector directly deposited on the back, as shown in Figure 1.

Because of their low surface coverage, the plasmonic nanostructures do not reflect all of the light reaching the back side of the stack and therefore need to be assisted by a back full surface reflector. Therefore, in addition to the plasmonic structures, we consider a full aluminum layer or a coating of TiO_2 nanoparticles to be used as back surface reflectors. Both structures are described in the succeeding text.

2.1.1. Back reflector scheme with plasmonic nanoparticles and full metal layer.

We use plasmonic metallic nanostructures to scatter the light, which is not absorbed in one pass, back toward the silicon, thanks to their preferential scattering characteristic. Silver was chosen as the material for plasmonic nanostructures based on the fact that it is less absorbing and has the plasmonic resonance in the desired wavelength range [20,21]. We choose silver nanodisks as a plasmonic

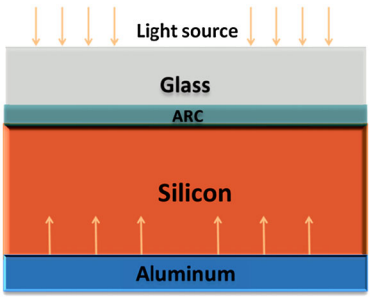

Figure 1. Reference structure with anti reflection coating and aluminum layer as back reflector.

nanostructure because of their higher scattering cross section [17]. The plasmonic back reflector scheme consists of a SiO_2 spacer layer adjacent to silicon, followed by a random or quasi-periodic array of silver nanodisks, a SiO_2 capping layer, and an aluminum coating as a back surface reflector (shown in Figure 2(a)). The reason we chose SiO_2 for the simulation study and the first experiments is that SiO_2 is a non-absorbing material that allows us to isolate the effect of the metal nanoparticles and back reflector.

However, for such thin c-Si layers, we generally choose to fabricate the solar cells work with amorphous silicon surface field and a-Si/c-Si heterojunctions, allowing the junction to be clearly defined, which would not be possible with a diffused surface field or junction emitter for example. This choice makes it more relevant to use ITO as an optical spacer and/or ARC layer. The index of ITO being slightly higher than SiO_2 (~1.8 instead of ~1.55) the phenomenology we study will not be deeply changed; the resonances will be slightly red shifted.

2.1.2. Back reflector scheme with plasmonic and dielectric nanoparticles.

A dielectric material with a high refractive index strongly reflects light, so we choose a titanium dioxide (refractive index ~2.73) nanoparticle coating as an alternative to an aluminum back surface reflector, taking advantage of both its good scattering and reflective properties [22]. Because simulating a back reflector scheme with densely packed dielectric nanoparticles of different sizes is not practical, we compare experimentally our concept of dielectric nanoparticle coating as shown in Figure 2 (b) with an aluminum layer, to be used as a back surface reflector for the back reflector scheme with plasmonic nanostructures.

2.2. Fabrication and characterization techniques

2.2.1. Fabrication of the 1 µm-c-Si on glass with intermediate anti reflection coating.

The 1-µm-thin c-Si films coated with a thin layer of SiN_x are fabricated by a layer-transfer process and are bonded on a glass carrier [20]. The c-Si film is first formed by the *empty-space-in-silicon-technique* [23], which consists of annealing above 1000 °C a wafer patterned with an array of cylindrical macropores that close, and eventually, all merge to form a thin overlaying film. In the present work, the thin film was formed by annealing at 1130 °C under 1 atm of H_2. After annealing, the suspended film was coated by a 40-nm layer of SiNx formed by plasma-enhanced chemical vapor deposition. It was then anodically bonded to a glass substrate by applying 1000 V at 320 °C. Finally, the film was detached from its parent wafer by pulling softly.

This technique is the only fabrication technique of such thin crystalline layer used in PV so far and is still under development in order to be made relevant for industrial application. We had to adapt the fabrication flow [19] in order to be able to process the rear side: the front side ARC had to be set between the glass substrate and the thin silicon layer, leading to difficulties in controlling its thickness, which is influenced by the bonding step. This thickness inaccuracy impacts the short wavelength part of the various measured spectra. However, as the part of the spectrum of interest for the back side reflector is here at wavelengths >500 nm, the ARC non-homogeneity does not interfere with the phenomena we are studying.

2.2.2. Fabrication of quasi-periodic silver nanodisks.

The quasi-periodic arrays of silver nanodisks have been fabricated by hole-mask colloidal lithography (HCL). This technique consists of the use of self-organized colloidal nanoparticles as a lithography mask for subsequent lift-off of metallic layers; it is described in detail in Reference [24]. A typical nanodisks arrangement exhibits short-range order, but no long-range order, as can be seen in Figure 3(a). We use here this technique at a small scale as we are making an optical study; however, this method is a reliable technique to produce 2D arrays of nanoplasmonic structures.

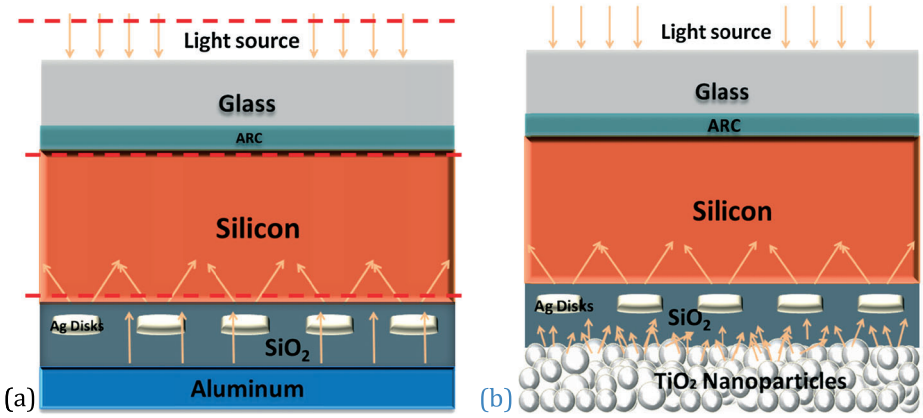

Figure 2. (a) Optical stack with plasmonic back reflector scheme in presence of (a) aluminum layer (b) dielectric nanoparticle coating, as back surface reflector. The red dashed lines in (a) shows the placement of monitors (in 3D simulations) for measuring absorption in different layers.

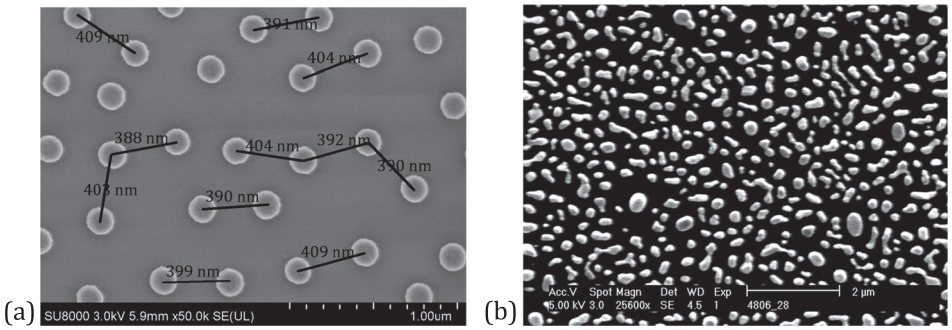

Figure 3. Scanning electron microscopy image of (a) the quasi-periodic array of nanodisks fabricated by hole-mask colloidal lithography and (b) the random array of Ag nanoparticles formed by thermal annealing of a Ag film on the optical stack.

2.2.3. Fabrication of random arrays of silver nanoparticles.

Random arrays of silver nanoparticles were fabricated on the basis of the coalescence of a thin metal film. A Ag film of thickness ~14 nm was deposited on an optical stack with the SiO_2 spacer layer already deposited and then annealed for 90 min under N_2 atmosphere at 220 °C. Annealing under the aforementioned conditions results out of thermal stress in the formation of a random array of silver nanoparticles, as shown in the scanning electron microscopy image in Figure 3(b). The size distribution is broader than for the HCL technique [25], making this technique easier to handle (and therefore to up-scale) but less precise; however, given the broad optical spectrum involved in c-Si photovoltaics (PV) and the importance of the cost aspect, this technique is also a candidate of choice for PV applications.

2.2.4. Fabrication of the dielectric nanoparticles coating.

The dielectric nanoparticles solution was prepared by dispersing TiO_2 nanoparticles (combination of particles sizes of 405, 320, and 220 nm) in propylene glycol methyl ether acetate. After dispersion, the glass plate (The glass substrate was a Corning Pyrex 7740 highly polished for anodic bonding purposes, with a roughness of 0.6 nm root mean square.) was dipped into the dielectric nanoparticle solution for 10 s followed by annealed for 20 min at 60 °C. The coating on the glass slide was used for comparing the reflection with the aluminum layer (also deposited on glass). For using in conjugation with the plasmonic nanoparticles, this coating was mechanically stacked on the back side of the structure.

2.2.5. Characterization.

We first characterized the particles by using scanning electron microscopy in order to check their size and spatial distribution. We then optically characterized the samples, allowing the deduction of the reflectance spectra of the various back reflectors studied, as well as the various stacks. We measured transmittance as well when relevant. These two measurements were performed using an integrating sphere and a light spot of 1 mm^2. They allowed us to deduce the absorption spectra. We used there an integrating sphere, which sums the reflection signal in the whole half space in front of the sample. The light incident on the sample was scanned from 400 to 1200 nm of wavelength, corresponding to the limits given both by the solar spectrum and silicon's absorption range.

2.3. Simulation setup

We chose the finite difference time domain [26] (FDTD) method and used a commercially available package, Lumerical FDTD solution [27], for simulating the optical behavior of our solar cell stack. 3D simulations were performed by using periodic boundary conditions in x and y dimensions to replicate the actual sample. Perfectly matched layer boundary conditions were used in the direction of propagation of light, that is, in z dimension, in order to account for the case that the light, which is not absorbed by the structure, is not reflected back in the simulation region. For high accuracy and detailed insight on the effect of parameters on the absorption throughout the chosen spectrum, the simulations were performed from 300 to 1200 nm with a wavelength step of 0.9 nm. The refractive index values for silicon, silver, silicon dioxide, and aluminum were taken directly from Lumerical database, whereas the refractive index of silicon nitride was measured using ellipsometry.

For calculating the absorption in any specific layer, the monitors were placed at the start and end of the layer (as shown by red dashed lines in Figure 2(a)). By calculating the difference in the amount of light entering and exiting the layer, we measured the absorption in that specific layer. Because a metal back surface reflector is present after the plasmonic back reflecting scheme, no light is crossing the simulation region in the $+z$ dimension, and all of the light that is not absorbed is reflected back. The absorption in the whole structure is calculated by subtracting the data collected from the motor placed before the source (as shown in Figure 2), from the amount of light falling into the substrate. This arrangement of monitor placement allows us to measure the absorption in the structure qualitatively and thus can be used to calculate it in any given layer.

The scattering behavior of the plasmonic nanostructure is a function of the distance of the particle from the high index medium (spacer layer), the dielectric function of the surrounding and nearby medium (material in which the particle is embedded), and the shape and size (height and diameter) of the nanoparticle itself. The resonance wavelength is also affected by interparticle spacing between nanodisks, which in the case of HCL samples is defined by electrostatic repulsion between charged colloidal beads [24]. Looking at the characteristic interparticle distances from Figure 3(a), and from the fact that using a period below 400 nm, results in very insignificant light trapping (as no light couples with silicon's higher order diffraction modes [28]), we choose 400 nm to be the interparticle spacing and optimized the other parameters. All of these parameters (shown in Figure 4) were optimized for maximizing absorption by the silicon layer.

The enhancement in absorption in silicon does not translate equally in an improved J_{sc} (short circuit current), as the incident solar spectrum is not flat and the energy of photons decreases with an increase in wavelength. To have qualitative insights on the effect of incorporation of the plasmonic back reflector scheme in the thin film cells, absorption is integrated over the AM1.5 solar spectrum so as to calculate the J_{sc} of the device using the equation in the succeeding text:

$$J_{sc\,\max} = \frac{q}{hc}\int_{300}^{1200} \lambda \times QE(\lambda) \times A(\lambda) \times S(\lambda) d\lambda \qquad (1)$$

where q is the elementary charge, λ is the wavelength, h is the Planck constant, c is the speed of light, QE is the quantum efficiency (collection efficiency in our case, as we are calculating absorption in the silicon layer only), S is the weighted sun spectrum (AM1.5 spectral irradiance), and A is the absorption in the material. Considering the collection efficiency in the silicon layer as unity, that is, assuming that every absorbed photon produces one charge carrier pair, the maximum achievable current J_{scmax} is calculated and is used as figure of merit for optimizing the parameters for the plasmonic back reflector.

2.3.1. Validation of simulations.

Minor inconsistencies between simulation and experiments can arise both in the trend and absolute value of the parameter under investigation because of various reasons. One of these is the fact that simulations consider a coherent light source, whereas the real coherence length is limited to a few microns. Secondly, the refractive indices of the materials were taken from Lumerical's data base, which can sometimes slightly differ from real values. Thirdly, the roughness of the surfaces and interfaces determines their reflection; in simulation, we choose perfect and flat surfaces, which is of course not the case experimentally. Finally, experiments always carry a certain degree of uncertainty in the thickness of the deposited material. Considering all these factors, before utilizing the simulations for studying and optimizing the parameters for back reflector schemes, we compare the results of simulations with the experiments to ascertain the degree of inconsistency. We choose two structures for the validation of simulations. The first structure consists only of a 1 μm thin c-Si layer on glass while the second structure is a 1 μm thin c-Si layer on glass with an aluminum back reflector. Despite the various factors that can result in any difference between the simulation and experimental data, our simulation results are within acceptable limits, as can be seen from the comparison in Figure 5(a) and (b). We attribute the slight discrepancies, mainly noticeable at short wavelength, to the error on the refractive index data, which was inputted into the model; but as this wavelength range is not our target, this will not impact our results.

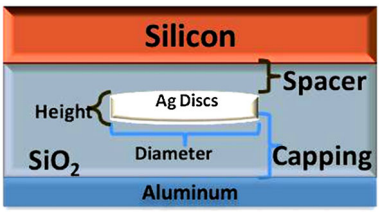

Figure 4. Parameters of the back reflector scheme optimized in this study.

3. SIMULATION RESULTS AND DISCUSSION

We scan hereafter the various relevant parameters of the plasmonic back reflector and extract a set of optimized parameters.

3.1. Optimization of plasmonic back reflector design with metal layer at the back

The dimensions of the nanodisks (height and diameter), the distance of plasmonic nanodisks from silicon (spacer layer), and the distance between the aluminum and the nanodisks (capping layer) (Figure 4) were scanned individually within 300–1200 nm wavelength range for maximizing the figure of merit, that is, the maximum achievable current. The absorption in the silicon layer was extracted for various values of parameters and J_{scmax} was calculated and compared. Spacer thickness of 13 nm, diameter of 205 nm, height of 55 nm, and capping layer 110 nm thick were chosen as starting parameters based on extrapolation of previous studies performed for the nanodisks situated at the front [16,29] and earlier calculations carried out for nanodisks situated at the back [30]. A first rough scan was performed, followed by a finer one, and results are presented here in the succeeding text.

3.1.1. Optimization of the capping layer.

The capping layer thickness influences the Fabry–Pérot (FP) cavity resonances, which are standing waves between the silicon surface and the metal back reflector. Depending

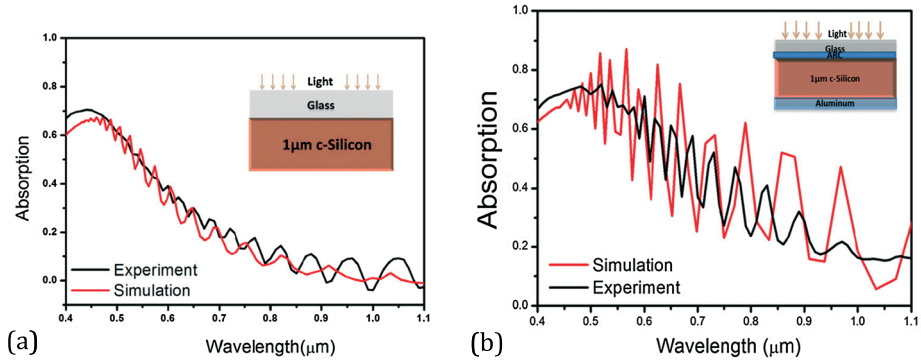

Figure 5. Comparison of experimental and simulation results for the absorption in the structure consisting of (a) silicon on glass (b) silicon on glass with anti reflection coating and aluminum as back surface reflector.

on the (spectral and spatial) positions of the minima and maxima of the field, it can enhance the absorption in the particles and the aluminum film or enhance the scattering efficiency of the metallic nanodisks. The ideal thickness cannot be chosen by considering only the FP modes, because the presence of particles strongly enhances the electric field in the region and thus changes the overall behavior, which is why we do not split the thickness study of the back dielectric layer from the nanoparticles (NPs) study. The thickness of the spacer was kept constant at 13 nm while the capping layer thickness was scanned form 100 to 560 nm, with a step of 20 nm. The upper limit of 560 nm was chosen in order to ensure the scanning of at least a free spectral range between the ground mode and the next resonance. A fine tuning was performed near the values of thicknesses, which gave maximum J_{scmax} enhancement. From the J_{scmax} curve shown in Figure 6(a), 210 nm of capping layer scatters the light into silicon most effectively and gives a J_{scmax} value of 24.76 mA/cm^2.

3.1.2. Height of the nanodisks.

When the disks are too thin, there is a high parasitic absorption, and when they are too thick, the plasmonic resonance wavelength for dipole oscillations red shifts

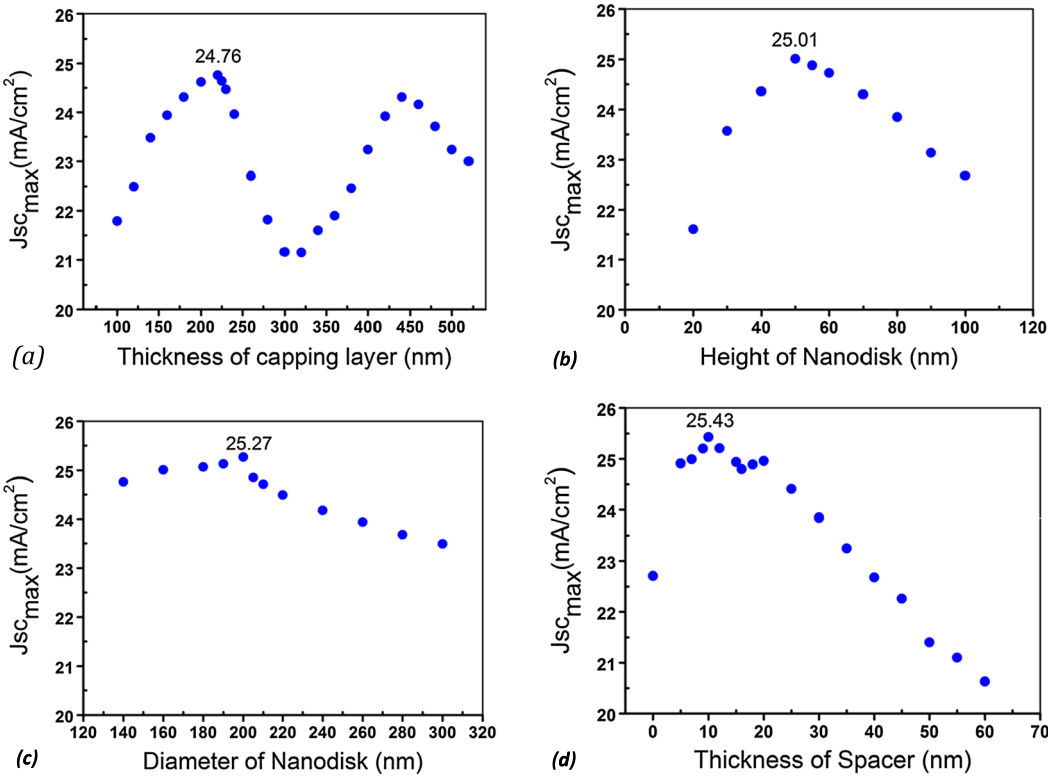

Figure 6. J_{scmax} values in function of various parameters: (a) thickness of capping layer, (b) height of nanodisk, (c) diameter of nanodisks, and (d) thickness of spacer.

and higher order modes appear at lower wavelengths [31]. The thickness of the nanodisks was scanned from 20 to 70 nm, for every 10 nm, while keeping the thickness of the capping layer constant at 210 nm. We observe that by decreasing the height of nanodisks below 50 nm, it decreases the scattering efficiency. Increasing the thickness of the nanodisks results in blue shifting of their surface plasmon resonance frequency. A 50 nm height of nanodisks scatters the light into silicon most effectively and gives a J_{scmax} value of 25.01 mA/cm^2.

3.1.3. Diameter of the nanodisks.

The diameter of silver nanodisks was scanned from 100 to 300 nm for every 20 nm, keeping their thickness constant at 50 nm, and the thickness of the capping the layer at 210 nm. Decreasing the diameter below 100 nm increases the Ohmic absorption rapidly as the particle size becomes too small with respect to the wavelength of incident light. For the particles with bigger diameter (~300 nm), the resonance shifts away from the desired part of the spectrum [31]. A 200 nm diameter of nanodisks scatters the light into silicon most effectively and gives a J_{scmax} value of 25.27 mA/cm^2.

3.1.4. Optimization of spacer layer.

With a thin spacer layer, the effect of silicon on the scattering properties of the plasmonic nanostructures will be maximum as, the closer the structure is to the high index medium, the higher is the effect on the homogeneity of its surrounding and hence on the preferential scattering properties. The effect of the spacers thickness was studied on the structure from 0 nm (i.e., nanodisks directly on the silicon) to 60 nm, for every 5 nm. The upper limit of 60 nm was chosen keeping in mind that after a few tens of nanometers, the effect of a nearby high index material on the scattering properties of the nanostructures decreases significantly, thus having negligible effect in the scattering pattern. A second scanning of thickness was performed near the values that gave the highest J_{scmax} values. A 10 nm of spacer layer results in the highest enhancement in the silicon layer with J_{scmax} value of 25.43 mA/cm^2. After the spacer thickness of ~20 nm, silicon's ability to modify the surrounding environment around the plasmonic particle starts decreasing and keeps on decreasing as the plasmonic nanostructure moves away from silicon. Another reason is the evanescent nature of the surface Plasmon field, which decreases very rapidly from the surface of the nanoparticle. Thus, the further the nanoparticle is from silicon, the weaker is the coupling of the enhanced field into the silicon. This can be seen from the decrease in the J_{scmax} values for the values higher than 20 nm in Figure 6(d) [32].

3.1.5. Summary of the parameter study and discussion.

We were able to achieve significant broadband enhancement, illustrated in Figure 7(a), that shows the comparison of absorption in silicon between the structure with the optimized back reflector scheme and the reference structure. Note that on the spectra shown on Figure 7, the absorption in silicon after 1170 nm should be zero as c-Si does not absorb light anymore; however, because of the necessary fit of the refractive index for FDTD simulations in the time domain, the absorption is artificially non-zero.

The $J_{sc\ max}$ is increased from 13.6 mA/cm^2 for the reference structure without ARC, and from 15.86 mA/cm^2 for the reference structure with ARC, to 25.43 mA/cm^2 for the structure with the optimized back reflector scheme and an ARC, which amounts to ~60.3% AM1.5 photon absorption enhancement in silicon. These results are summarised in Table I. We also compare the absorption enhancement in the silicon layer by comparing the number of photons absorbed from the real AM1.5 solar spectrum (Figure 7(b)); this gives both a qualitative and a quantitative aspect of absorption enhancement.

By comparing the red curve (optical stack with optimized plasmonic back reflector scheme) with the blue curve (reference solar cell structure), we clearly see that there is broadband enhancement in absorption throughout the spectrum, especially from ~550 to 1100 nm.

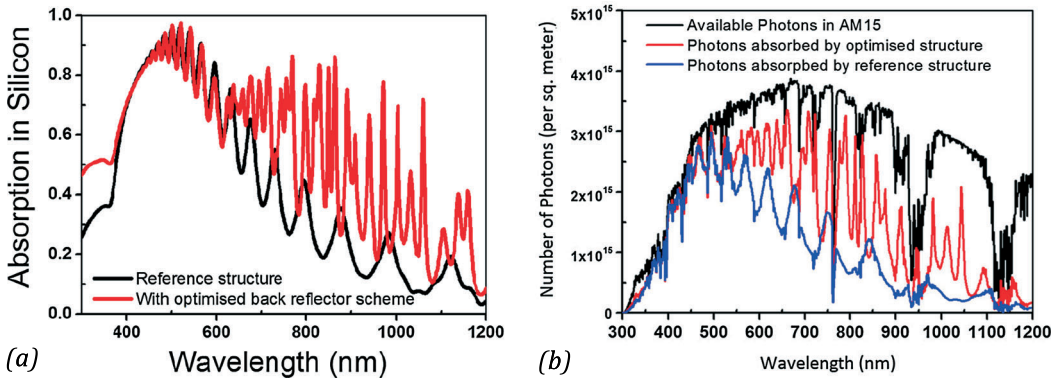

Figure 7. (a) Integrated absorption in silicon with optimized back reflector (black) and reference structure (red). The difference in short wavelength is due to a numerical artifact. (b) Number of photons absorbed in the silicon layer in the reference structure (red) and in the optimized plasmonic solar cell structure (blue). The black curve shows the number of photons present at AM1.5 conditions.

3.2. Absorption in metal back reflector

There is always a significant parasitic/Ohmic absorption (light which is absorbed by the structure and does not result in charge carrier generation), both in the plasmonic nanostructures and the metal layer which is used as back surface reflector. We cannot avoid the parasitic absorption in our plasmonic nanodisks beyond a certain limit as we have already optimized the parameters to maximize the useful absorption. But we can still minimize parasitic absorption in the aluminum layer that is used as flat back reflector layer. We can quantify this absorption in the aluminum layer in combination with the plasmonic nanostructures. The parasitic absorption in the presence and absence of the flat aluminum back reflecting layer is compared in Figure 8(a). We clearly see a high amount of absorption in the system combining nanodisks and aluminum layer as back surface reflector. This suggests that the presence of the aluminum layer may enhance the parasitic absorption in the plasmonic nanoparticles, via coupling of the exponentially decaying field of the metal film with the Plasmon modes of the nanoparticles embedded in dielectric [33]. To have further insight, we compare the absorption in the nanodisks in presence and absence of a flat aluminum layer, as shown in Figure 8(b). We also quantify the absorption in the aluminum layer alone as shown in Figure 8(c).

The comparisons clearly show that there is almost no enhancement of the parasitic absorption in the plasmonic silver nanodisks by adding the flat aluminum layer. The major fraction of the light in the wavelength range of 550–850 nm is lost because of the parasitic absorption in the flat aluminum layer. Essentially, what happens is that the nanoparticles scatter light to the region with the largest photonic density of states (or the largest index). Silicon has a large index, but the surface plasmons on the Al surface also have a large effective index. The closer we put the Al to the particles, the more effective the coupling between the particles and the Al layer. This explains that the extra absorption will take place in the Al, not in the Ag particle. If we can avoid this loss and redirect this light into the silicon, we will considerably enhance absorption in silicon.

Table I. Summary of the maximal achievable currents obtained after a coarse and fine scanning of the nanoparticles parameters, for the single reference layer as well as two back reflector conditions.

Structure	J_{scmax} (mA/cm^2)
Reference	15.9
Reference with ARC	18.4
Structure with ARC and optimized back surface reflector	26.9

ARC, anti reflection coating.

3.2.1. Replacing aluminum with perfect metal boundary.

We now simulate the structure with an optimized back reflector scheme and replace the aluminum layer by a perfect metal (using metal as boundary condition in $+z$ direction). This metal boundary condition means 100% reflection and no parasitic absorption. This allows giving an idea of the possible gain, which would be brought by a non-absorbing reflector behind the nanoparticles. Figure 9 compares absorption in silicon with the aluminum layer and with a perfect metal (non-absorbing) layer as back surface reflector.

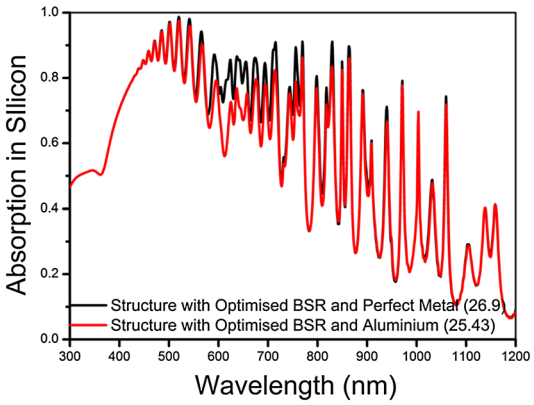

Figure 9. Absorption in silicon with a perfect metal (black) and an aluminum layer (red) on the back.

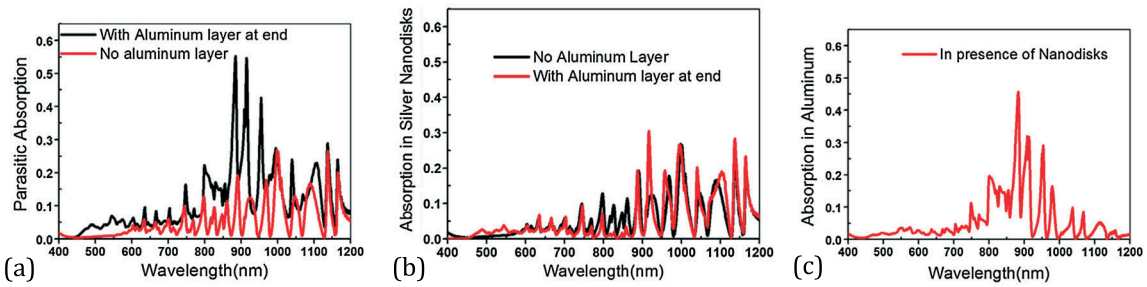

Figure 8. (a) Parasitic absorption in the presence (black) and absence (red) of aluminum layer but always with nanoparticles on the back, (b) absorption in the silver nanodisks in presence (black) and the absence (red) of aluminum layer, and (c) absorption in the aluminum mirror(back surface reflector) in presence of silver nanodisks. In both the case, the capping is 210 nm thick, height of nanodisks is 50 nm, and diameter of nanodisks is 200 nm and spacer thickness in 10 nm.

As there is no absorption in a perfect metal, the light, which was previously lost because of these parasitic absorption in aluminum, is sent back toward silicon, hence increasing absorption in the silicon layer. One can see that this happens at the plasmonic resonance, which corresponds to the maximum in parasitic absorption in the metal stack (Figure 8(a) and (c)) The structure with the optimized back reflector scheme with a perfect reflector gives a J_{scmax} of 26.9 mA/cm^2, whereas with an aluminum layer as back surface reflector, the J_{scmax} is 25.43 mA/cm^2. Thus, by using a perfect metal as back surface reflector with plasmonic nanoparticles, we were able to further enhance the maximum achievable current by ~69.6%.

4. EXPERIMENTAL RESULTS AND DISCUSSION

4.1. Experimental characterization of the numerical optimal

After validation of our model with the reference optical stack (Section 2.3.1), we now validate our simulations for the plasmonic back reflector scheme. We fabricated the plasmonic back reflector scheme on the back side of a 1 μm thin c-Si layer with nanodisks of height 50 nm, ~200 nm diameter, ~15 nm spacer, and capping 100 nm. The absorption in the structure was compared with the simulated results, shown in Figure 10.

Simulation and experiments are in good agreement. The difference at short wavelengths in the experimental and simulation data can reasonably be attributed to the previously discussed refractive index discrepancy. Another major factor is that in the simulations, the interparticle spacing was fixed to be 400 nm, while in the experiment, it varies with ±20 nm (as seen in Figure 3(a)); this yields sharper resonances in the red part of the simulated spectrum.

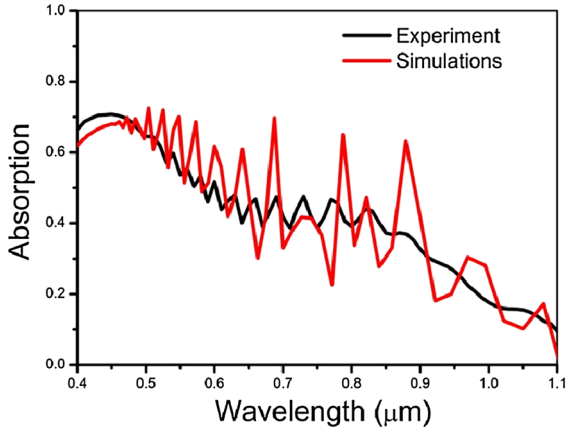

Figure 10. Comparison of absorption in the structure with the plasmonic back reflector scheme without a metal layer at the back: simulations (red) and experiment (black).

4.2. Beyond the numerical optimal: using dielectric nanoparticles coating as a back reflector

Absorption in the aluminum layer in the back reflector scheme is significant and is highly undesirable as it lies mainly in the wavelength region of interest. In order to overcome this, we have seen previously that a perfect metal would be ideal, although of course not available. However, a flat reflector, ideal or not, can have the drawback of enhancing the coupling between the FP cavity and the plasmon modes, which is the cause of this high absorption in the back reflector, as can be seen from Figure 8(c). Therefore, beyond having an ideal reflector, a loss of coherence would help avoiding any interference and therefore any kind of coupling between the light reflected by the back reflector and by the plasmonic behavior of the nanostructures. This can be achieved if the reflection from the back surface reflector is not specular but diffuse. Therefore, we propose to replace the metal layer in the back reflector scheme by a coating of dielectric nanoparticles, which will scatter back light thanks to Mie scattering [34], the resulting structure is shown in Figure 2(b). For diffused scattering of light throughout the spectrum, we chose a combination of three different particle sizes of titanium dioxide, that is, 405, 320, and 220 nm in order to achieve scattering on a broad spectral range.

From Figure 11, we see that the dielectric nanoparticles coating scatters ~80% of the reflected light compared with ~10% for a flat metallic back reflector, thanks to the Lambertian nature of the reflection profile. Thus, it is very effective in randomizing the direction of light that is reflected back into the silicon and should enhance absorption as compared with the aluminum layer. The fact that the reflected light is diffuse is expected to avoid any coupling between the plasmon resonance and cavity modes between the silicon and the flat metallic back surface reflector.

4.3. Experimental comparison of optimized back reflection schemes

We fabricated the cell stack with an optimized back reflector scheme, following the simulations presented, for optical characterization. We chose to fabricate this optical demonstrator with ITO surrounding the metal nanoparticles instead of SiO_2, keeping in mind the future need for contact formation in actual devices that, with such a thin c-Si layer, need to be a-Si/c-Si heterojunction solar cells, therefore needing a transparent and conductive oxide as an optical spacer and antireflection coating. The index of ITO being slightly higher than SiO_2 (~1.8 instead of ~1.55) the phenomenology we study will not be deeply changed as explained in Section 2.1.

The various parameters of the back reflecting stack are aimed to correspond to the results of the numerical optimisation within the experimental uncertainties. We tried two sets of nanoparticles: quasi-periodic and random plasmonic nanoparticles. The particles fabricated by the HCL

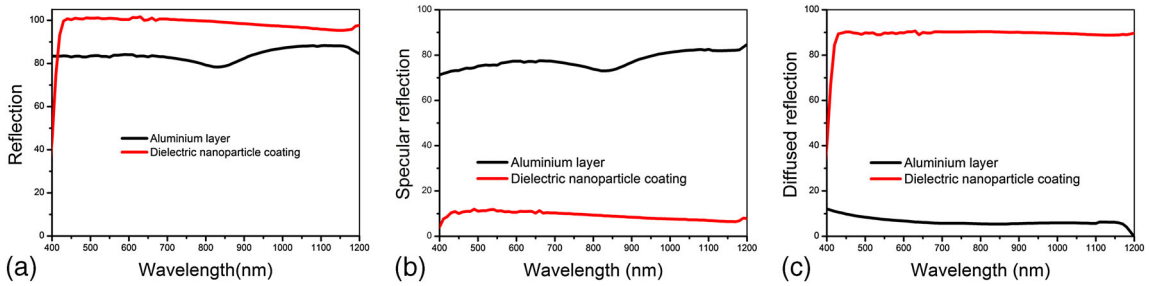

Figure 11. Comparison among different components of reflection from the aluminum layer (black) and the dielectric nanoparticle coating (red): (a) full reflection, (b) specular part of reflection, and (c) diffuse part of reflection.

process have a diameter of ~200 nm and an interparticle distance of ~400 nm, while the particles fabricated by an anneal step have a broad size distribution. Figure 12 compares the absorption for the structure without any back reflector (which will from now be used as a reference), the structure with quasi-periodic nanoparticles, and finally with random nanoparticles.

Absorption measurements in the structure without back surface reflector show expected results. The stacks with nanoparticles on the back show an enhanced absorption, thanks both to the scattering and reflective behavior of the nanoparticles. The higher absorption in the stack with fully random (annealed) particles can be attributed both to the higher surface coverage (as can be seen on Figure 3(b)) and to the broader scattering region because of the broader size distribution. The difference in absorption in wavelength below 500 nm is due to the difference in thickness of ARC because of experimental errors as explained earlier and not related to the back reflector.

In order to demonstrate the scattering character of the plasmonic particles, and to differentiate it from a simple reflector with a partial surface coverage, we proceed in two ways:

(1) We add a metallic planar back reflector on the back of the planar structure without nanoparticles (green curve in Figure 12) and compare it with the structures with the nanoparticles. One can observe that the absorption of the planar structure is enhanced thanks to a doubling of the optical path length of the red and near-infrared photons, causing a proportional enhancement of the absorption in this spectral range. On the other hand, the structures with nanoparticles show a non-constant increase of absorption showing a scattering resonance acting mainly in the red-near-infrared spectral region.

(2) We showed earlier the matching of the experimental and simulated optical properties of the structure with nanoparticles. The latter shows that having metal nanoparticles on the back helps further enhancing the absorption of a silicon active layer. This confirms that our fabricated nanoparticles are behaving as the simulated nanoparticles and not as a planar back reflector.

In order to avoid transmission losses, we have proposed to add an aluminum layer as back surface reflector on the back of the nanoparticles. Again, absorption measurements show as expected, in Figure 13, that absorption in the

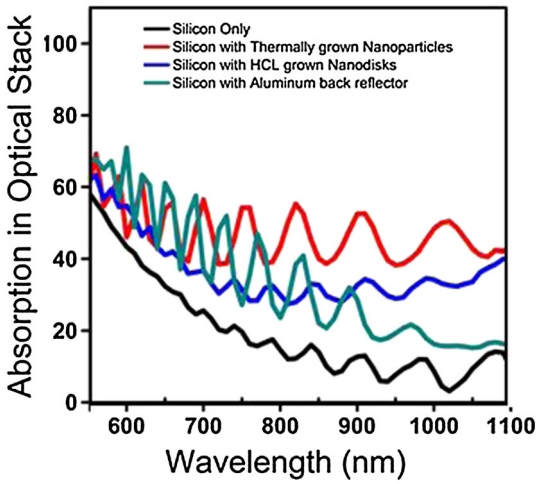

Figure 12. Absorption in the optical stack with anti reflection coating (black) silicon only, (blue) silicon with hole-mask colloidal lithography grown nanodisks only, and (red) silicon with thermally grown nanoparticles.

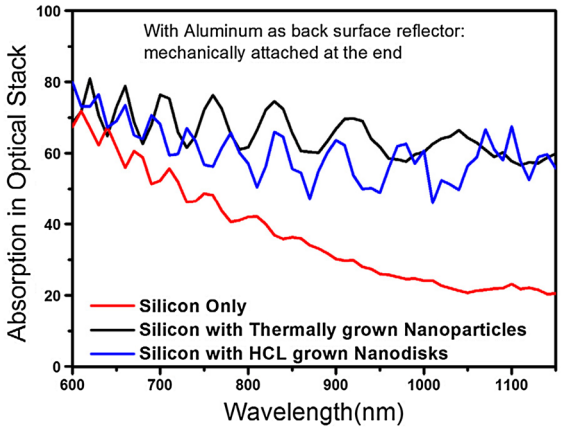

Figure 13. Absorption in optical stack in silicon only (black), with random plasmonic nanostructure (red) and with quasi-periodic plasmonic nanodisks (blue). In all cases, detached aluminum is used as back surface reflector.

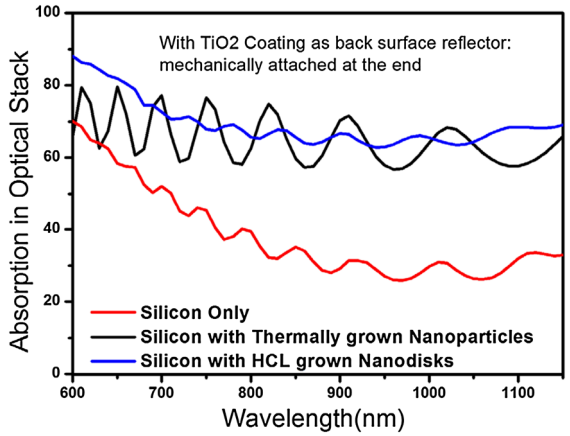

Figure 14. Absorption in optical stack in silicon only (black), with random plasmonic nanostructure (red) and with quasi-periodic plasmonic nanodisks (blue). In all cases, a dielectric nanoparticles coating is used as back surface reflector.

structure is highest for the case with random nanoparticles, then for quasi-periodic nanoparticles, and minimum for the reference structure.

We showed in the simulation (Section 3.2) that there is some absorption in the metals and in particular in the Al mirror; this is confirmed on Figure 13 by the absorption at wavelengths reaching the c-Si bandgap, due mostly to metals as c-Si absorbs very little at such wavelengths. We also discussed the potentialities of a back reflector based on dielectric nanoparticles, we now compare the previous structures with a stack having the dielectric nanoparticles coating as back reflector. We obtain a similar result, with a smaller difference between the two kinds of nanoparticles. It is thus likely that part of the supplementary absorption in the case of the annealed random particles was due to enhanced parasitic absorption in the back reflector.

The dielectric nanoparticles coating is known to act as a randomly patterned surface. Figure 14 shows the absorption of the stack with a simple TiO_2 back reflector and then with the metal nanoparticles sandwiched between the TiO_2 and the silicon. The presence of the metal NPs further enhances absorption in silicon, showing that they scatter light beyond the scattering of a random pattern. As for Figure 13, the parasitic absorption in metals is also visible here when reaching c-Si's bandgap (for wavelengths above 1170 nm)

We finally compare the performances of the various optimized back reflectors: simple metal, nanoparticles with metal back reflector, and metal nanoparticles with a dielectric nanoparticles back reflector. One can see that the overall absorption of the structure is the highest with the last combination (a stack of dielectric and metallic nanoparticles), whereas we have shown in this study that the absorption of the dielectric nanoparticles is negligible. This means that the optimal stack that we deduced in simulation is indeed further improved by the use of a scattering dielectric back reflector.

5. CONCLUSION

We studied the effect of plasmonic nanoparticles shape, size, and embedding materials on their scattering behavior. We then optimized a complete solar cell back reflector scheme by combining plasmonic and dielectric nanoparticles and were able to achieve 69.6% of J_{scmax} enhancement in simulations when comparing with a typical stack with a planar back reflector and a back reflector with plasmonic and dielectric nanoparticles. We can safely conclude based on simulations, and experimental validation of our simulations, that incorporation of nanodisks of optimized parameters in the back reflector scheme, along with a perfect reflector as back surface reflector, results in broadband absorption enhancement in ultra-thin c-Si layer. The optimized structure has a spacer thickness of 10 nm, silver nanodisks of height 50 nm, diameter 200 nm, and capping layer of thickness 210 nm. We also show that using a dielectric nanoparticles coating as back reflector further enhances scattering from the plasmonic back reflector and also avoids any parasitic absorption loss and should therefore be preferred to a metallic back reflector. We believe that this work paves the way to having an optimal back reflecting scheme for thin c-Si PV cells.

ACKNOWLEDGEMENTS

This work was performed in the frame of the European FP7 project PRIMA grant agreement number 248154. The authors would like to acknowledge fruitful discussions with Sven Leyre (Katholieke Hoge School Ghent).

REFERENCES

1. Green MA. Limits on the open-circuit voltage and efficiency of silicon solar cells imposed by intrinsic Auger processes. *Electron Devices, IEEE Transactions on* 1984; **31**: 671–678. DOI: 10.1109/T-ED.1984.21588
2. Queisser HJ. Photovoltaic conversion at reduced dimensions. *Physica E: Low-dimensional Systems and Nanostructures* 2002; **14**: 1–10. ISSN 1386–9477, DOI: 10.1016/S1386-9477(02)00353-3
3. Campbell P, Green MA. Light trapping properties of pyramidally textured surfaces. *Journal of Applied Physics* 1987; **62**: 243–249. DOI: 10.1063/1.339189
4. Sai H, Kanamori Y, Arafune K, Ohshita Y, Yamaguchi M. Light trapping effect of submicron surface textures in crystalline Si solar cells. *Progress in Photovoltaics: Research and Applications* 2007; **15**: 415–423. DOI: 10.1002/pip.754
5. Gordon I, Carnel L, Van Gestel D, Beaucarne G, Poortmans J. 8% Efficient thin-film polycrystalline-silicon solar cells based on aluminum- induced crystallization and thermal CVD. *Progress in Photovoltaics:*

Research and Applications 2007; **15**: 575–586. DOI: 10.1002/pip.765

6. Trompoukis C, El Daif O, Depauw V, Gordon I, Poortmans J. Photonic assisted light trapping integrated in ultrathin crystalline silicon solar cells by nanoimprint lithography. *Applied Physics Letters* 2012; **101**: 103901. DOI: 10.1063/1.4749810
7. Faraday M. On the color of colloidal gold. *Philosophical Transactions. Royal Society of London* 1857; **147**: 145–181.
8. Mie G. Beiträge zur Optik trüber Medien, speziell kolloidaler Metallöungen. *Annalen der Physik* 1908; **25**: 377–445.
9. Kreibig U, Vollmer M. *Optical Properties of Metal Clusters*. Springer-Verlag: Berlin, Heidelberg, 1995.
10. Catchpole K, Polman A. Plasmonic solar cells. *Optics Express* 2008; **16**: 21793–21800.
11. Catchpole KR, Polman A. Design principles for particle plasmon enhanced solar cells. *Applied Physics Letters* 2008; **93**: 191113–191113-3. DOI: 10.1063/1.3021072
12. Niesen B, Rand BP, Van Dorpe P, Cheyns D, Shen H, Maes B, Heremans P. Near-field interactions between metal nanoparticle surface plasmons and molecular excitons in thin-films. Part I: absorption. *Journal of Physical Chemistry C*, Article ASAP DOI: 10.1021/jp305892e
13. Mertz J. Radiative absorption, fluorescence, and scattering of a classical dipole near a lossless interface: a unified description. *Journal of the Optical Society of America B* 2000; **17**: 1906–1913.
14. El Daif O, Tong L, Figeys B, Jain S, Miljkovic VD, Depauw V, Vercruysse D, Van Nieuwenhuysen K, Dmitriev A, Van Dorpe P, Gordon I, Dross F. Silver nanodiscs for light scattering in thin epitaxial silicon solar cells: influence of the disc radius. *Materials Research Society Symposium Proceedings* 2012; **1391**. DOI: 10.1557/opl.2012.527
15. Atwater HA, Polman A. Plasmonics for improved photovoltaic devices. *Nature Materials* 2010; **9**: 205–213. DOI: 10.1038/nmat2629
16. Spinelli P, Hebbink M, de Waele R, Black L, Lenzmann F, Polman A. Optical impedance matching using coupled plasmonic nanoparticle arrays. *Nano Letters* 2011; **11**(4)*:* 1760–1765. DOI: 10.1021/nl200321u
17. Yu ET, Derkacs D, Matheu P, Schaadt DM. Plasmonic nanoparticle scattering for enhanced performance of photovoltaic and photodetector devices. *Proceedings SPIE 7033, Plasmonics: Nanoimaging Nanofabrication, and Their Applications IV* 2008; **70331V**. DOI: 10.1117/12.798327
18. Depauw V, Qiu Y, Van Nieuwenhuysen K, Gordon I, Poortmans J. Epitaxy-free monocrystalline silicon thin film: first steps beyond proof-of-concept solar cells. *Progress in Photovoltaics: Research and Applications* 2011; **19**: 844–850. DOI: 10.1002/pip.1048
19. Depauw V, Gordon I, Beaucarne G, Poortmans J, Mertens R, Celis J-P. Large-area monocrystalline silicon thin films by annealing of macroporous arrays: understanding and tackling defects in the material. *Journal of Applied Physics* 2009; **106**: 033516. DOI: 10.1063/1.3183942
20. Ru EL, Etchegoin P. *Principles of Surface Enhanced Raman Spectroscopy*. Elsevier: Oxford, U.K., 2009, 978-0-444-52779-0
21. Rycenga M, Cobley CM, Zeng J, Li W, Moran CH, Zhang Q, Qin D, Xia Y. Controlling the synthesis and assembly of silver nanostructures for plasmonic applications. *Chemical Reviews* 2011; **111**: 3669–3712.
22. Berger O, Inns D, Aberle AG. Commercial white paint as back surface reflector for thin-film solar cells. *Solar Energy Materials & Solar Cells* 2007; **91**: 1215–1221.
23. Sato T, Mizushima I, Taniguchi S, Takenaka K, Shimonishi S, Hayashi H, Hatano M, Sugihara K, Tsunashima Y. Fabrication of silicon-on-nothing structure by substrate engineering using the empty-space-in-silicon formation technique. *Japanese Journal of Applied Physics* 2004; **43**: 12–18.
24. Fredriksson H, Alaverdyan Y, Dmitriev A, Langhammer C, Sutherland DS, Zäch M, Kasemo B. Hole–mask colloidal lithography. *Advanced Materials* 2007; **19**: 4297–4302. DOI: 10.1002/adma.200700680
25. Beck FJ, Mokkapati S, Catchpole KR. Plasmonic light-trapping for Si solar cells using self-assembled, Ag nanoparticles. *Progress in Photovoltaics: Research and Applications* 2010; **18**: 500–504. DOI: 10.1002/pip.1006
26. Shlager KL, Schneider JB. A selective survey of the finite-difference time-domain literature. *Antennas and Propagation Magazine, IEEE* 1995; **37**: 39–57.
27. Lumerical Solutions, Inc. http://www.lumerical.com/tcad-products/fdtd/, Accessed: 16 June 2014
28. Wang E-C, Mokkapati S, Soderstrom T, Varlamov S, Catchpole KR. Effect of nanoparticle size distribution on the performance of plasmonic thin-film solar cells: monodisperse versus multidisperse arrays. *Photovoltaics, IEEE Journal of* 1–4. DOI: 10.1109/JPHOTOV.2012.2210195
29. Figeys B, El Daif O. Exploring the parameter space of disc shaped silver nanoparticles for thin film silicon photovoltaics, arXiv:1111.3791 [cond-mat.mes-hall]
30. El Daif O, Depauw V, Jain S, Gordon I, Dross F, Van Dorpe P, Trompoukis C, Catchpole K, De Keersmaecker K, Ristow A. Plasmon back side light-scattering for thin crystalline silicon solar cells, poster, Photovoltaic Technical Conference 2012, Congress center of Aix-en-Provence, France.

31. El Daif O, Tong L, Figeys B, Van Nieuwenhuysen K, Dmitriev A, Van Dorpe P, Gordon I, Dross F. Front side plasmonic effect on thin silicon epitaxial solar cells. *Solar Energy Materials and Solar Cells* 2012; **104**: 58–63.
32. Lim SH, Mar W, Matheu P, Derkacs D, Yu ET. Photocurrent spectroscopy of optical absorption enhancement in silicon photodiodes via scattering from surface plasmon polaritons in gold nanoparticles. *Journal of Applied Physics* 2007; **101**: 104309.
33. Maier SA, Atwater HA. Plasmonics: localization and guiding of electromagnetic energy in metal/dielectric structures. *Journal of Applied Physics* 2005; **98**(1): 011101–011101-10. DOI: 10.1063/1.1951057
34. Cotter JE, Hall RB, Mauk MG, Barnett AM. Light trapping in silicon-film solar cells with rear pigmented dielectric reflectors. *Progress in Photovoltaics: Research and Applications* 1999; **7**: 261–274.